Model for complex heart rate dynamics in health and diseases

Kiyoshi Kotani,[1] Zbigniew R. Struzik,[2] Kiyoshi Takamasu,[3] H. Eugene Stanley,[4] and Yoshiharu Yamamoto[2]
[1]*Graduate School of Information Science and Technology, The University of Tokyo, 7-3-1 Hongo, Bunkyo-ku, Tokyo 113-8656, Japan*
[2]*Educational Physiology Laboratory, Graduate School of Education, The University of Tokyo, 7-3-1 Hongo, Bunkyo-ku, Tokyo 113-0033, Japan*
[3]*Department of Precision Engineering, Graduate School of Engineering, The University of Tokyo, 7-3-1 Hongo, Bunkyo-ku, Tokyo 113-8656, Japan*
[4]*Center for Polymer Studies and Department of Physics, Boston University, Boston, MA 02215, USA*
(Received 3 June 2005; published 5 October 2005)

A physiologically motivated, dynamical model of cardiovascular autonomic regulation is shown to be capable of generating long-range correlated and multifractal heart rate. *Virtual disease* simulations are carried out systematically to account for the disease-induced relative dysfunction of the parasympathetic and the sympathetic branches of the autonomic control. Statistical agreement of the simulation results with those of real life data is reached, suggesting the possible use of the model as a state-of-the-art basis for further understanding of the physiological correlates of complex heart rate dynamics.

DOI: 10.1103/PhysRevE.72.041904 PACS number(s): 87.19.Hh, 87.80.Vt, 89.75.Da, 05.45.Df

I. INTRODUCTION

The complexity of biological dynamics with long-range (multi-)scaling properties continues to attract the interest of the scientific community, while the origins and the nature of this type of biocomplexity have yet eluded satisfactory explanation. This is partly because proposed models [1,2] for biocomplexity cover exclusively spatially interacting phenomena, leaving the dynamical complexity [3] to a large degree unexplored. A model involving an explicit temporal axis is needed better to understand how the complex biological dynamics arises.

Healthy human heart rate is a typical example of signals showing long-range temporal correlations [4,5] and multifractal scaling properties [6,7]. Physiologically, the origin of the complex dynamics of heart rate has been attributed to antagonistic activity of the two branches of the autonomic nervous system: the parasympathetic (PNS) and the sympathetic (SNS) nervous systems, respectively, decreasing and increasing heart rate [4,5,7,8]. There also exist physiological models for the dynamics of the neural regulation of heart rate [9,10], equipped with antagonistic and multiplicative delayed feedback loops. The purpose of the present study is to examine whether a state-of-the-art, nonlinear, and physiologically sound model is capable of displaying complex dynamics with long-range (multi-)scaling properties.

The breakdown of the complex heart rate dynamics has also been reported in illness associated with altered cardiovascular autonomic regulation. There is evidence that decreased long-range correlated fluctuations [11,12], especially in the low frequency region [11,13], are associated with increased mortality in cardiac patients and the multifractality of heart rate dynamics is lost in patients with congestive heart failure [6]. Further, a recent study by Struzik *et al.* [14] systematically showed that the disease-induced relative dysfunction of either the PNS or the SNS results in more correlated heart rate dynamics, but only the PNS dysfunction leads to reduced multifractality.

In the present study, we also examine whether the model proposed allows one to simulate disease-specific alterations in heart rate complexity by changing the model parameters responsible for controlling the autonomic activity. Long-range (multi-)scaling properties of ambulatory heart rate have recently been shown to be highly independent of behavioral effects (e.g., transient exercise, diet, postural changes, etc.) [7,15] and to provide robust indicators of autonomic abnormality due to the disease per se [14]. *Virtual disease* simulations will therefore likely be important in advancing an understanding of the physiological correlates of complex heart rate dynamics and in diagnosing the conditions of a range of patients having abnormality in their autonomic regulation.

II. DESCRIPTION OF MODEL

The model (Fig. 1) is a system of delay-differential equations based on the one proposed by Seidel and Herzel [9] and later modified by Kotani *et al.* [10] to incorporate additional factors needed to simulate synchronization between heartbeat and respiration [16]. In this study, we further refine the model to account for the effects of sympathetic efferent activity on cardiac filling, which is important for the maintenance of normal blood pressure. We also choose to omit the nonlinear phase effectiveness curve in the original model [9] because the results are not altered without this additional nonlinearity. In summary, the model consists of physiological factors including: (i) Neural afferents from blood pressure sensors, i.e., baroreceptors, to the central nervous system; (ii) autonomic (sympathetic and parasympathetic) neural efferents from the brain stem cardiovascular centers; (iii) mechanical signal transduction within the cardiovascular system finally setting the arterial blood pressures; and (iv) the effect of the baroreceptor afferents on the instantaneous phase of the respiratory oscillator.

The baroreceptor activity ν_b is set by blood pressure p (mm Hg; 0.133 kPa) and its first derivative as

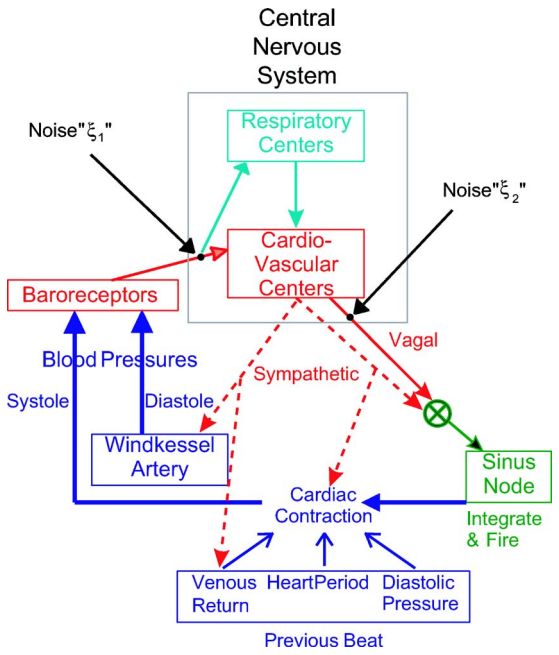

FIG. 1. (Color online) Schematic diagram of the cardiovascular/respiratory model in this study. The diversity in the model is caused mainly by factors such as time delays in the neural conduction, multiplications in neural and mechanical variables, and time-varying Windkessel dynamics.

$$\nu_b = k_1(p - p^{(0)}) + k_2\frac{dp}{dt} + \xi_1 \tag{1}$$

(default parameters: $k_1=0.02$ mm Hg^{-1}, $k_2=1.25\times10^{-3}$ s mm Hg^{-1}, and $p^{(0)}=50.0$ mm Hg). The ξ_1 is a mechanical noise added to the blood pressure signal on a beat-to-beat basis. We use a Brownian motion updated at each heartbeat and held within interbeat periods. The standard deviation of ξ_1 is set to 0.16.

This ν_b subsequently determines the efferent sympathetic neural activity (ν_s), after being modulated by respiratory influence R, as

$$\nu_s' = \nu_s^{(0)} - k_s^b\nu_b + k_s^r(1-R) \tag{2}$$

[$\nu_s^{(0)}=0.95$, $k_s^b=0.8$, and $k_s^r=3\times10^{-4}$] and

$$\nu_s = \nu_s'[\tanh(\nu_s'\times 100) + 1.0]/2.0. \tag{3}$$

The hyperbolic tangent function is used to prevent negative neural activity, i.e., negative firing frequency. Likewise, the parasympathetic neural activity (ν_p) is determined as

$$\nu_p' = k_p[\nu_p^{(0)} + k_p^b\nu_b + k_p^r(1-R) + \xi_2] \tag{4}$$

($k_p=1.1$, $\nu_p^{(0)}=0.0$, $k_p^b=0.036$, and $k_p^r=4.5\times10^{-3}$) and

$$\nu_p = \nu_p'[\tanh(\nu_p'\times 100) + 1.0]/2.0. \tag{5}$$

The ξ_2 is the (central) neuronal noise affecting the parasympathetic activity on a beat-to-beat basis. We use a fractional Brownian motion with a global Hurst exponent of zero (i.e., $1/f$ noise) of which the standard deviation is set to 0.012. The $1/f$ noise in heart rate dynamics is indeed thought to be of central origin, because it is reported [17,18] to be lost during deep sleep, when central nervous system activity is considered to be minimal.

The heartbeat is generated by an integrate-and-fire model: When the pacemaker phase (ϕ) of the sinus node hits the threshold of 1.0, the pacemaker fires and ϕ is immediately reset to zero. The phase velocity is a function of both sympathetic (f_s) and parasympathetic (f_p) influences on the sinus node

$$\frac{d\phi}{dt} = \frac{1}{T^{(0)}}f_s f_p \tag{6}$$

($T^{(0)}=0.6$ s), and the sympathetic (facilitatory) influence f_s is a function of the cardiac concentration ($c_{c\mathrm{Ne}}$) of the sympathetic neurotransmitter "norepinephrine" (Ne)

$$f_s = 1 + k_\phi^{c\mathrm{Ne}}\left[c_{c\mathrm{Ne}} + (\hat{c}_{c\mathrm{Ne}} - c_{c\mathrm{Ne}})\frac{(c_{c\mathrm{Ne}})^{n_{c\mathrm{Ne}}}}{(\hat{c}_{c\mathrm{Ne}})^{n_{c\mathrm{Ne}}} + (c_{c\mathrm{Ne}})^{n_{c\mathrm{Ne}}}}\right] \tag{7}$$

($k_\phi^{c\mathrm{Ne}}=1.6$, $\hat{c}_{c\mathrm{Ne}}=2.0$, and $n_{c\mathrm{Ne}}=2.0$). As the release of Ne by the neural input ν_s is known to have slow kinetics, the $c_{c\mathrm{Ne}}$ kinetics is described, after incorporating the neural conduction delay ($\theta_{c\mathrm{Ne}}=1.65$ s), by the first-order model

$$\frac{dc_{c\mathrm{Ne}}}{dt} = -\frac{c_{c\mathrm{Ne}}}{\tau_{c\mathrm{Ne}}} + k_{c_{c\mathrm{Ne}}}^s\nu_s(t-\theta_{c\mathrm{Ne}}) \tag{8}$$

($\tau_{c\mathrm{Ne}}=2.0$ s and $k_{c_{c\mathrm{Ne}}}^s=0.7$).

The parasympathetic (inhibitory) influence f_p assumes no transmitter kinetics, because the kinetics of the neurotransmitter "acetylcholine" is sufficiently fast, and the f_p is a direct function of the neural input ν_p. Thus, we have

$$f_p = 1 - k_\phi^p\left[\nu_p(t-\theta_p) + (\hat{\nu}_p - \nu_p(t-\theta_p))\times\frac{\nu_p(t-\theta_p)^{n_p}}{(\hat{\nu}_p)^{n_p} + \nu_p(t-\theta_p)^{n_p}}\right] \tag{9}$$

($\theta_p=0.5$ s, $k_\phi^p=5.8$, $\hat{\nu}_p=2.5$, and $n_p=2.0$).

The systolic part of the blood pressure for each heartbeat is determined by the diastolic pressure of the previous beat d_{i-1} (mm Hg) and the cardiac contractility of the current beat S_i

$$p = d_{i-1} + S_i\frac{t-t_i}{\tau_{\mathrm{sys}}}\exp\left(1 - \frac{t-t_i}{\tau_{\mathrm{sys}}}\right), \tag{10}$$

where t_i is the time of last contraction onset and $\tau_{\mathrm{sys}}=0.125$ s. The hypertensive factor S_i is a function of the duration of the previous heartbeat period T_i (s) through the Frank-Starling mechanism (i.e., greater cardiac filling results in greater contractility), of the cardiac concentration of Ne [Eq. (8)] through an increase in cardiac contractility, and of the vascular concentration of Ne ($c_{v\mathrm{Ne}}$) through the increased venous return to the heart. This is described by

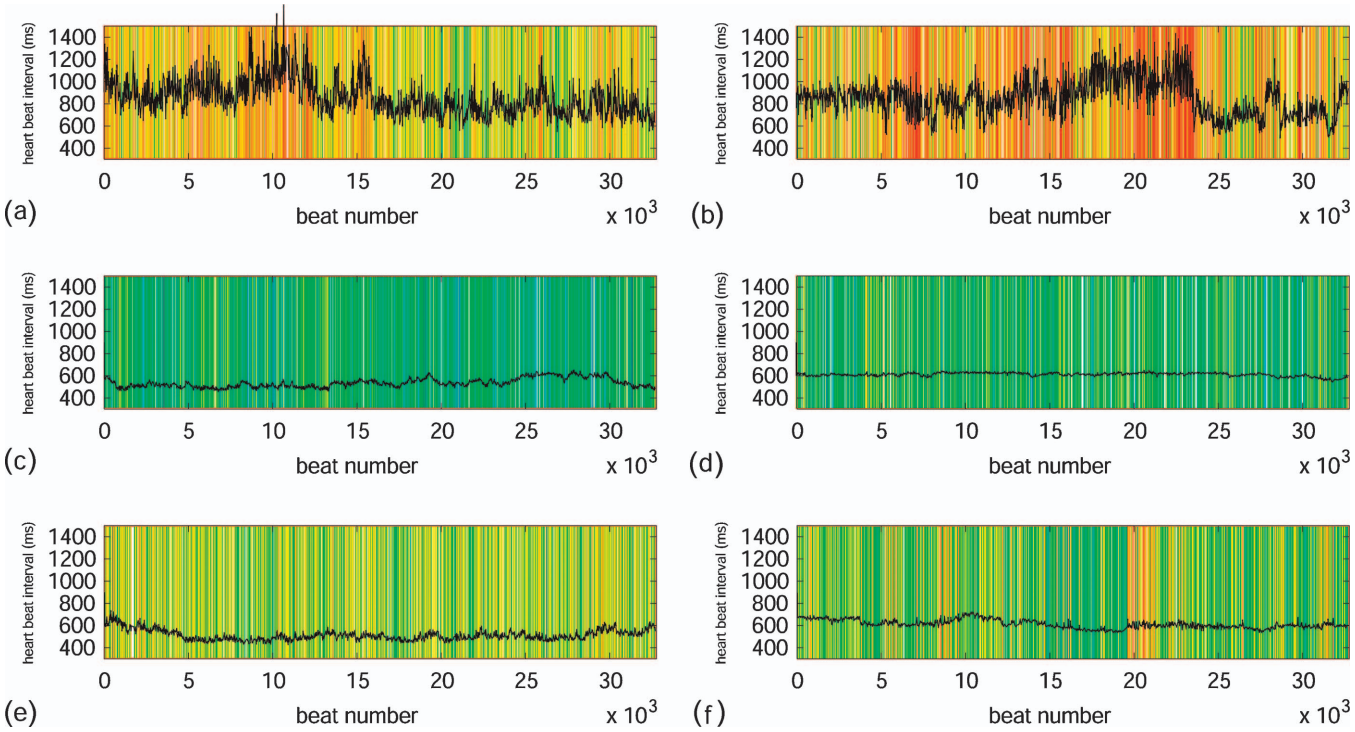

FIG. 2. (Color) Heartbeat intervals from representative simulations (a), (c), and (e) and the actual data (b), (d), and (f) with a color bar of the local Hurst exponent. The strongest singularity is red ($h=0.0$), and the weakest singularity is blue ($h=0.6$). The data of each panel is as follows: (a) Virtual heartbeats mimicking healthy subjects; (b) actual heartbeats of healthy subjects; (c) virtual heartbeats mimicking subjects who suffer from CHF; (d) actual heartbeats of subjects who suffer from CHF; (e) virtual heartbeats mimicking subjects who suffer from PAF; and (f) actual heartbeats of subjects who suffer from PAF.

$$S_i' = S^{(0)} + k^c_{Sc_{c\mathrm{Ne}}} + k^t_S T_{i-1} + k^v_{Sc_{\upsilon\mathrm{Ne}}} \tag{11}$$

($S^{(0)}=-13.8$ mm Hg, $k^c_S=10$ mm Hg, $k^t_S=45$ mm Hg s^{-1}, and $k^v_S=20$ mm Hg) and

$$S_i = S_i' + (\hat{S} - S_i')\frac{S_i'^{n_S}}{S_i'^{n_S} + \hat{S}^{n_S}} \tag{12}$$

($\hat{S}=70$ mm Hg and $n_S=2.5$).

The diastolic part of the blood pressure is described by the relaxation of the Windkessel arteries with a time-varying relaxation "constant" τ_v (s)

$$\frac{dp}{dt} = -\frac{p}{\tau_v(t)}, \tag{13}$$

and the τ_v is a function of the vascular concentration of Ne ($c_{\upsilon\mathrm{Ne}}$) as

$$\tau_v = \tau_v^{(0)} - \bar{\tau}_v\left[c_{\upsilon\mathrm{Ne}} + (\hat{c}_{\upsilon\mathrm{Ne}} - c_{\upsilon\mathrm{Ne}})\frac{(c_{\upsilon\mathrm{Ne}})^{n_{\upsilon\mathrm{Ne}}}}{(\hat{c}_{\upsilon\mathrm{Ne}})^{n_{\upsilon\mathrm{Ne}}} + (c_{\upsilon\mathrm{Ne}})^{n_{\upsilon\mathrm{Ne}}}}\right] \tag{14}$$

($\tau_v^{(0)}=2.8$ s, $\bar{\tau}_v=1.2$ s, $\hat{c}_{\upsilon Ne}=1.0$, and $n_{\upsilon\mathrm{Ne}}=1.5$). As in Eq. (8), the $c_{\upsilon\mathrm{Ne}}$ has first-order kinetics with the conduction delay $\theta_{\upsilon\mathrm{Ne}}$ (s)

$$\frac{dc_{\upsilon\mathrm{Ne}}}{dt} = -\frac{c_{\upsilon\mathrm{Ne}}}{\tau_{\upsilon\mathrm{Ne}}} + k^s_{c_{\upsilon\mathrm{Ne}}}[\nu_s(t-\theta_{\upsilon\mathrm{Ne}}) + k_\upsilon] \tag{15}$$

($\tau_{\upsilon\mathrm{Ne}}=2.0$ s, $k^s_{c_{\upsilon\mathrm{Ne}}}=0.5$, and $k_\upsilon=0.2$), where k_υ is a constant ensuring the tonic firing of the sympathetic nerve to the vascular smooth muscles. According to Seidel and Herzel [9], an increase in the vascular sympathetic delay $\theta_{\upsilon\mathrm{Ne}}$ to 4.2 s leads via a Hopf bifurcation to low-frequency ($\approx$0.1 Hz), sustained heart rate and blood pressure oscillations. Thus, we adopt this value as $\theta_{\upsilon\mathrm{Ne}}$ in the present study.

To incorporate cardio-respiratory interaction, we first introduce an instantaneous phase of respiration r where $0.0<r\leqslant 0.5$ and $0.5<r\leqslant 1.0$, respectively, correspond to expiratory and inspiratory periods. With this r, the respiratory influences R in Eqs. (2) and (4) are described by

$$R = \cos(2\pi r). \tag{16}$$

Without the influence of baroreceptor afferents, the r has a constant phase velocity of:

$$\frac{dr}{dt} = \frac{1}{T_{\mathrm{resp}}}, \tag{17}$$

where T_{resp} is a constant respiratory period.

Next we add the effect of the baroreceptor afferents on the respiratory phase: if $\nu_b > \nu_{\mathrm{trig}}$ during expiration $[\sin(2\pi r)>0.0]$, the r is modulated as

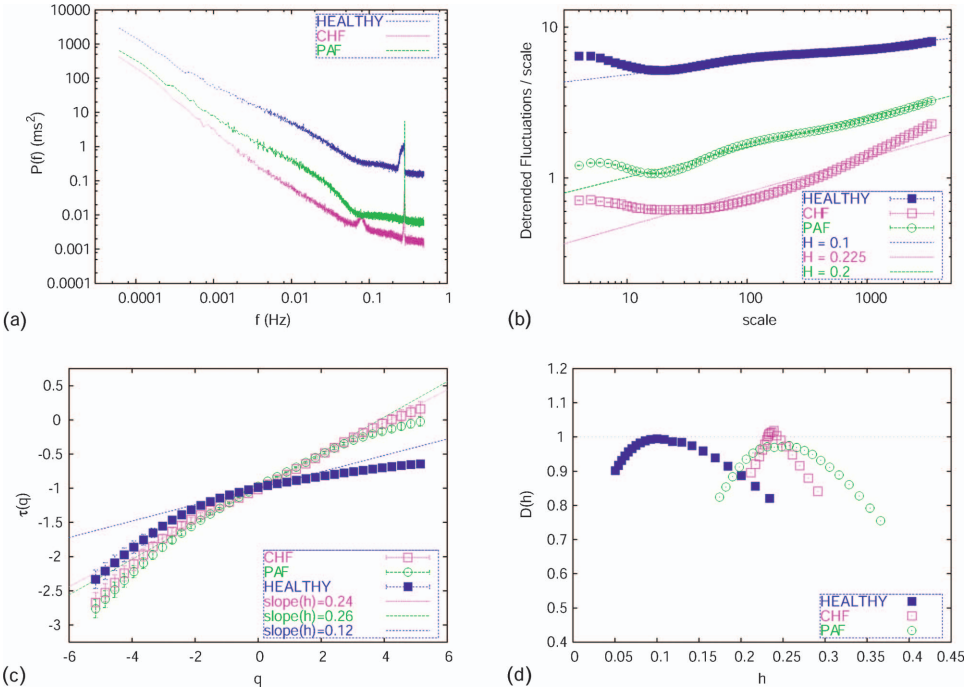

FIG. 3. (Color) Averaged results of 50 simulations mimicking the healthy, CHF, and PAF states. (a) Power spectra; (b) DFA plot; (c) multifractal spectra $[\tau(q)]$; and (d) singularity spectra $[D(h)]$.

$$\frac{dr'}{dt} = \frac{1}{T_{\text{resp}}} - G \times (\nu_b - \nu_{\text{trig}}), \tag{18}$$

and:

$$\frac{dr}{dt} = \frac{dr'}{dt}\left[\tanh\left(\frac{dr'}{dt} \times 100\right) + 1.0\right]/2.0, \tag{19}$$

where $T_{\text{resp}}=3.5$ s is a constant respiratory period and $G=0.2$ and $\nu_{\text{trig}}=1.3$ are constant values. The lower bound of respiratory phase velocity dr/dt is set to 0.0 to prevent "reverse" breathing. Note that higher ν_b results in slower phase velocity during expiration, and thus lengthens the period of expiration as observed in experimental studies [19,20].

III. SIMULATION AND DATA ANALYSIS

A set of delay-differential equations is numerically integrated by the fourth-order Runge-Kutta method with a constant step size (5 ms). To handle the time delays, we use ring buffers which store the immediate history. In all simulations, we skip the first 180 s to exclude transients, and analyze the following 50 000 heartbeat intervals, applying the procedures described below.

Heartbeat interval data are resampled at a frequency of 1 Hz and the power spectrum is calculated by fast Fourier transform (FFT), after applying the Bingham's cosine tapered window.

To evaluate the long-range temporal correlations of beat-to-beat heartbeat intervals [4,5], the global Hurst exponent is calculated by second-order detrended fluctuation analysis (DFA) [21]. The integrated time series $y(k)$ is divided into boxes whose size is n. In each box, the variance $F^2(n)$ after the second-order detrending is calculated as $F^2(n)=1/n\Sigma_{k=1}^{n}[y(k)-y_n(k)]^2$, where $y_n(k)$ is the second-order least-squares fit of $y(k)$ within the box. The fluctuation function $F(n)$ is the average root-mean-square of all the boxes. Scaling exponent α is obtained by the relation $F(n)\sim n^{\alpha}$, and the global Hurst exponent by $H=\alpha-1.0$. The range of $1.7<\log n<3.0$ is used to calculate the α.

The multifractal scaling properties of heart rate [6,7] are evaluated by using multifractal formalization, applying wavelet theory [22] to calculate the scaling exponents $\tau(q)$ by a power-law dependence $Z_q(a)\sim a^{\tau(q)}$, where the *partition function* $Z_q(a)$ is the sum of the qth powers of the local maxima of the absolute moduli of the wavelet transform coefficients at scale a. In this study, the third derivative of the Gaussian function is used as the analyzing wavelet. We use $1.3<\log a<2.7$ to calculate $\tau(q)$. This $\tau(q)$ is then related to $D(h)$ through a Legendre transform [23], $D(h)=qh-\tau(q)$, where $h=d\tau(q)/dq$: $D(h_o)$ is the fractal dimension of the subset of the original time series characterized by the local (Hurst) scaling exponent h_o [23]. We use an average curvature of $\tau(q)$ [i.e., $\Delta^2\tau(q)/\Delta q^2$] for $-3<q<3$ as a multifractal index; more negative values imply greater multifractality.

IV. VIRTUAL PHYSIOLOGY EXPERIMENTS

By setting $(k_p,k^s_{c_{\text{cNe}}},k^s_{c_{\text{tNe}}})=(1.1,0.7,0.5)$, where k_p, $k^s_{c_{\text{cNe}}}$ and $k^s_{c_{\text{tNe}}}$, respectively, stand for the central PNS gain, and SNS gains for the cardiac and vascular branches, the model produces a heartbeat interval sequence [Fig. 2(a)] that is similar to actual data for a young healthy individual [Fig. 2(d)], taken from a previous study [15]. With these parameters, the power spectrum shows a distinct high-frequency peak indicative of the presence of respiratory modulation of the heart rate at around 0.3 Hz, a small low-frequency peak at around 0.1 Hz, due to the emergence of a limit cycle caused by the vascular sympathetic delay (θ_{tNe}), and a $1/f$-type characteristic in the lower frequency region [Fig.

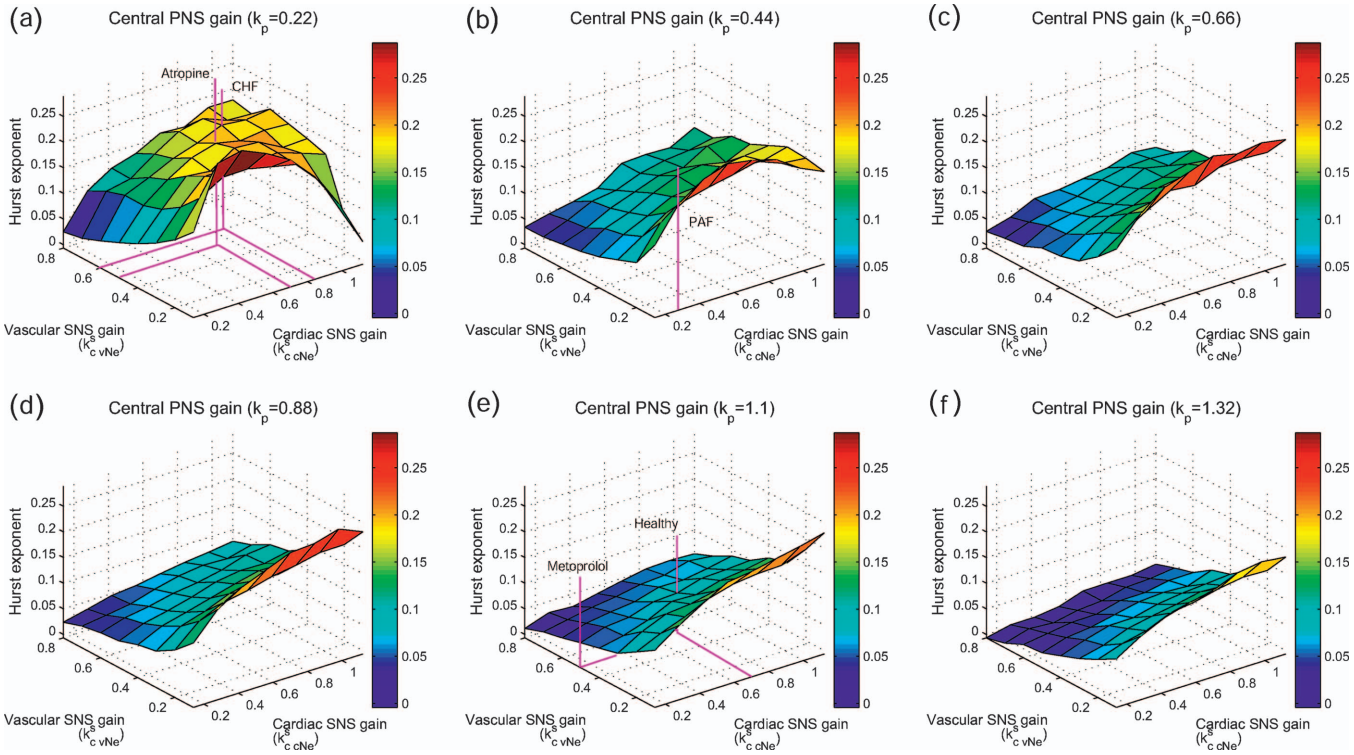

FIG. 4. (Color) Average global Hurst exponent as functions of cardiac ($k^s_{c_{c\mathrm{Ne}}}$) and vascular ($k^s_{c_{v\mathrm{Ne}}}$) sympathetic activity at different levels of vagal or parasympathetic (k_p) activity.

3(a)], all reported in actual heartbeat intervals in healthy individuals [5].

The DFA plot [Fig. 3(b)] also shows that there are long-range temporal correlations with the average global Hurst exponent approximating 0.1, again consistent with the value reported for healthy subjects [14]. In addition, we observe a nonlinear, curved multifractal spectrum $\tau(q)$ [Fig. 3(c)] and a wide singularity spectrum $D(h)$ [Fig. 3(d)], implying multifractal heartbeat interval fluctuations mimicking those in healthy humans [6,7]. When we examine the local contribution to multifractality by using the method of local effective Hurst exponent [24], it is observed that nonuniform distributions of the local Hurst exponent are indeed similar for the simulation [Fig. 2(a), color coding] and the data [Fig. 2(d)].

Although there have been various cardiovascular models hitherto proposed to account for some of the statistical properties observed in actual human heart rate, such as high- and low-frequency periodicities [9,25] and global long-range correlations [3], ours is the first one that can generate all of the known statistical properties of heartbeat interval fluctuations, up to higher moment statistics probed by multifractal spectra. In other words, our physiological model is able to account, in a statistical sense, for most of the variability components observed in tens of thousands of heartbeats. Note, in addition, this model is capable of exhibiting yet another nonlinear phenomenon, namely, the cardiorespiratory synchronization [16], as reported in Ref. [10].

Nunes Amaral *et al.* [7] recently studied multifractal properties of the heartbeat under pharmacological suppression of either the PNS or the SNS in humans. They found that, by the administration of *atropine*, a blocker for the acetylcholine receptor at the heart, influencing the PNS function, the multifractality of the heartbeat was greatly reduced (converted to monofractal signals) and the global Hurst exponent was significantly increased. By contrast, the administration of *metoprolol*, a blocker for the β-adrenergic receptor at the heart, but not for the α-adrenergic receptor at the vascular smooth muscles, only influencing the cardiac SNS function, resulted in almost unchanged, albeit slightly decreased, multifractality, with the global Hurst exponent unaltered.

Our model is capable of reproducing these experimental results. For instance, when we move the parameter settings for the healthy, unblocked state to $(k_p, k^s_{c_{c\mathrm{Ne}}}, k^s_{c_{v\mathrm{Ne}}}) = (0.22, 0.7, 0.5)$, i.e., only decreasing the central PNS gain k_p, this *virtual* administration of *atropine* results in an increased global Hurst exponent [Figs. 4(a) and 4(e)], and greatly reduced multifractality [Figs. 5(a) and 5(e)]. By contrast, the *virtual* administration of *metoprolol*, by only reducing the cardiac SNS gain $k^s_{c\mathrm{Ne}}$ to $(k_p, k^s_{c_{c\mathrm{Ne}}}, k^s_{c_{v\mathrm{Ne}}}) = (1.1, 0.14, 0.5)$, does not change either the global Hurst exponent [Fig. 4(e)] or the multifractality index [Fig. 5(e)] dramatically.

It is of note that the surfaces for both the average global Hurst exponent (Fig. 4) and the multifractality index (Fig. 5), drawn after large-scale (20 times) simulations with various combinations of $(k_p, k^s_{c_{c\mathrm{Ne}}}, k^s_{c_{v\mathrm{Ne}}})$, are far from monotonic, indicating that the effects of the central PNS, cardiac SNS, and vascular SNS gains are not additive, and interact with each other in a complex manner. For example, with the presence of sufficient central PNS gains, increasing cardiac SNS gain generally results in an increased Hurst exponent [Figs. 4(d)–4(f)], but such a response is not observed with the re-

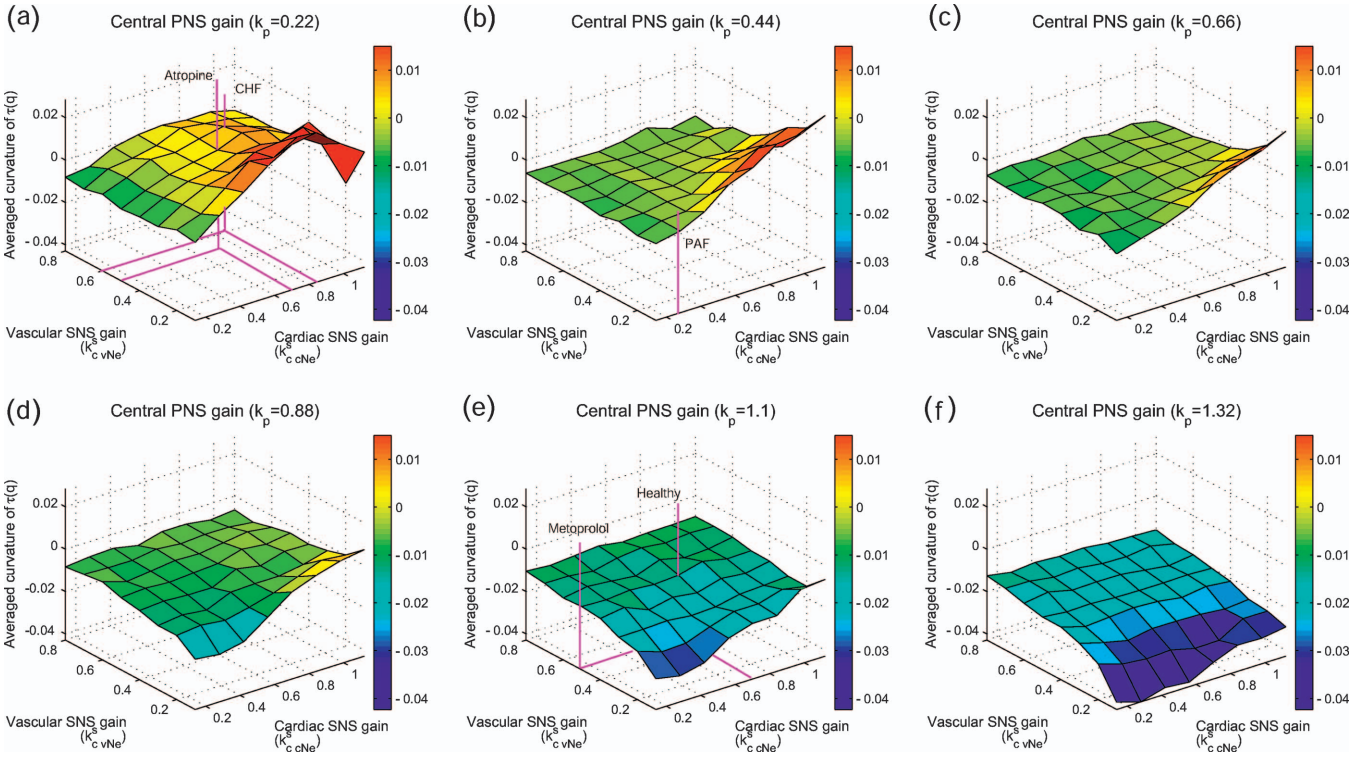

FIG. 5. (Color) Multifractality by the averaged curvature of $\tau(q)$ as functions of cardiac ($k^s_{c_{cNe}}$) and vascular ($k^s_{c_{vNe}}$) sympathetic activity at different levels of vagal or parasympathetic (k_p) activity. The negative values imply greater multifractality.

duced central PNS gain [Fig. 4(a)]. Also, the effects of SNS gains on the multifractal indices are exaggerated only with moderate (or natural) levels of central PNS gain [Figs. 5(e) and 5(f)]. These interactions seem to be important in understanding changes in heart rate complexity in pathological conditions, as described in the next section.

V. VIRTUAL DISEASES

Congestive heart failure (CHF) and primary autonomic failure (PAF) are diseases for which the long-range (multi-)scaling properties of large-scale heart rate have been rigorously examined to date [6,14]. CHF is a severe heart disease associated with decreased PNS [26,27] and increased SNS [26,28] activity. It has been reported that the heart rate dynamics of CHF patients is characterized by increased long-range correlations (an increase in the global Hurst exponent) and decreased multifractality [6]. PAF, by contrast, is a neurological disease where neuronal degeneration of the autonomic nervous system, especially in SNS, is the main pathology [29]. Thus, in the case of PAF, both PNS and SNS activity are suppressed and the rate of suppression is greater in the SNS than in the PNS. It has been reported that the heart rate dynamics of PAF patients is characterized by increased long-range correlations but preserved multifractality [14].

In the simulations, we heuristically choose the parameter sets of $(k_p, k^s_{c_{cNe}}, k^s_{c_{vNe}})$ for CHF and PAF as (0.22, 0.84, 0.6) and (0.44, 0.28, 0.1), respectively. Compared with the setting $(k_p, k^s_{c_{cNe}}, k^s_{c_{vNe}}) = (1.1, 0.7, 0.5)$ for the healthy case, there is a considerable decrease in the PNS gain (k_p) and an increase in the cardiac ($k^s_{c_{cNe}}$ through the β-adrenergic mechanisms), and in the vascular ($k^s_{c_{vNe}}$ through the α-adrenergic mechanisms) SNS gains for CHF (Figs. 4 and 5). For PAF, while the decrease in k_p is moderate, both the cardiac and the vascular SNS gains are greatly reduced (Figs. 4 and 5).

The virtual CHF results in a considerable decrease in both the mean heart interbeat interval and in heart rate variability [Fig. 2(b)], comparable with an actual record for a CHF patient [Fig. 2(e)]. Both the power spectrum [Fig. 3(a)] and the DFA plot [Fig. 3(b)] show steeper slopes in the low frequency or the long-range region, indicative of stronger long-range correlations than in the virtual healthy case; the increase of long-range correlations in CHF is well evidenced [4,6]. The $\tau(q)$ spectrum has a linear dependence on q [Fig. 3(c)] that results in a narrow singularity [$D(h)$] spectrum [Fig. 3(d)], implying the reduced multifractality reported in actual CHF [6]. This is also reflected in the monochromatic color bars for the local Hurst exponents [Fig. 2(b)] similar to those observed for actual CHF patients [Fig. 2(e)] [14].

The virtual PAF also results in considerable decreases in both the mean interbeat interval and heart rate variability [Fig. 2(c)], compared with healthy cases, but not to the level for CHF. As reported previously [14], the global Hurst exponent estimated by the DFA slope is higher than that for the virtual healthy case [Fig. 3(b)]. However, the $\tau(q)$ spectrum shows a comparable nonlinear dependence on q in the healthy case [Fig. 3(c)], which results in a wider $D(h)$ spectrum [Fig. 3(d)], implying the preserved multifractality reported in actual PAF [14]. The color bars for the local Hurst

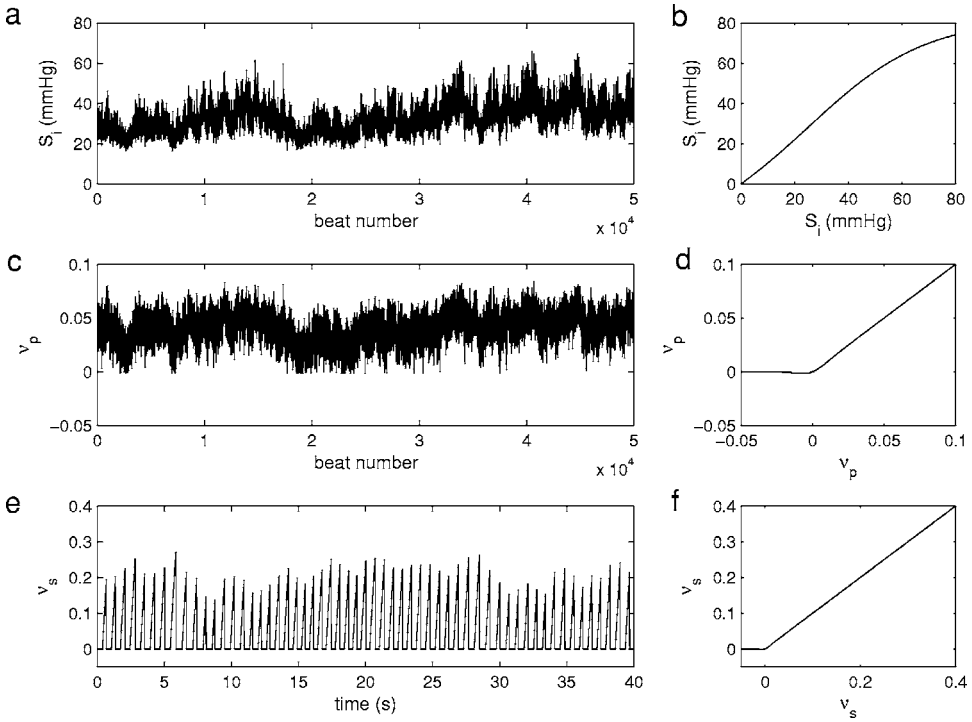

FIG. 6. (a) Time series of S_i; (b) its sigmoidal function as Eq. (12). Time series of S_i is lower than 60 mm Hg most of the time, and in this region the sigmoidal function is linear. Therefore, the nonlinear effect of this function is very small; (c) ν_p when a heartbeat occurs; (d) its sigmoidal function as Eq. (5). At around 20 000 beats, the ν_p is bounded by the sigmoidal function, but this state is temporal; (e) time series of ν_s during 40 s; (f) its sigmoidal function as Eq. (3). Normally, sympathetic nervous activity ν_s crosses the sigmoidal threshold almost consistently, which is the same as the simulation by Seidel and Herzel [9]. Simulated data of (a), (c), and (e) are performed within the parameters of the healthy condition.

exponents [Fig. 2(c)] are indeed heterogeneous, like those observed for actual PAF patients [Fig. 2(f)] [14].

The surfaces for both the average global Hurst exponent (Fig. 4) and the multifractality index (Fig. 5) drawn after large-scale simulations with various combinations of $(k_p, k^s_{c_{c\mathrm{Ne}}}, k^s_{c_{\nu\mathrm{Ne}}})$ generally show that the global Hurst exponent increases with the reduced central PNS gain, increased cardiac SNS gain, and reduced vascular SNS gain. Also, the multifractality index increases when the central PNS gain is higher and the vascular SNS gain is lower, but remains unrelated with the cardiac SNS gain. Changes in heart rate complexity in illness associated with altered cardiovascular autonomic regulation like CHF and PAF might be caused by a combination of these factors.

VI. DISCUSSION

We have presented a physiological dynamical model of cardiovascular autonomic regulation which is shown to be capable of generating a long-range correlated and multifractal heart rate signal. A stochastic feedback model was previously proposed [3] to account only for the long-range correlations of heart rate. Our model shares some similarity with this stochastic feedback model, in that a system with feedback, autonomic regulation is driven by stochastic noise. However, our model is equipped with fundamental physiological mechanisms leading to altered long-range correlations and multifractality of heart rate in health, in pharmacological interventions, and in disease.

Indeed, our model captures the general statistical and transient characteristics of, respectively, the global and local Hurst exponents, which reflect the long-range correlations present in the system, subject to autonomic (im)balance. Further, we compare the multifractality index of the healthy simulation data with that of surrogate data having the same Fourier amplitudes and distributions as the original data [30]. We confirm that the multifractality in our model is significant at the level of $P<0.001$ by a paired t test. Also, it is of note that the model produces nontrivial Hurst exponents between 0.0 and 0.5, i.e., between those of monofractal noise sources used to drive the system, that change consistently with experimental and disease-induced alternations in the autonomic nervous system.

Our measurements were conducted using the same methodology for both the simulated model time series and the human heart rate data sets. Therefore, while the precise meaning of the term "multifractal heart rate" is still open to investigation, we conclude that we have succeeded in qualitatively reproducing the observed heterogeneity of the local Hurst exponents and their relative contributions to the multifractal spectra in both the data and model simulations.

Arguably, the model includes many built-in nonlinearities, which can potentially lead to nonlinear complexity of the simulated heart rate. The use of the nonlinear functions is based on the phenomenological physiological knowledge. For instance, sigmoidal non-linearities [Eqs. (3), (5), (8), (10), (12), (15), and (19)] are considered to be observed in the actual cardiovascular system with the role of avoiding nonphysiological (i.e., too large and/or too small) values. It has to be noted, however, that in our simulation, essentially only the linear part of most of these functions is used and the nonlinear effect of these functions seems very small. Figure 6 shows two examples of the relation between a sigmoidal function and output data. In both variables of S_i and ν_p, the nonlinear effect of the sigmoidal function indeed seems to be small. An exception is the sympathetic nervous activity ν_s [Eq. (3)], which crosses the sigmoidal threshold consistently. This effect, also reported in the original simulation of Seidel and Herzel [9], is considered physiological because the sym-

pathetic activity is generally burstlike. Also, such consistent crossing does not result in a temporally long-range correlated and multifractal heart rate signal. Therefore, the multifractality of human heartbeat in our model is mainly generated by resting components such as antagonistic dual controls by the SNS and PNS, delayed and time-variant feedback, multiplication in the sinus node, and mixing and circulation of noise. We believe these findings should prove to be helpful in clarifying the mechanism(s) of multifractality in actual human heartbeat.

VII. CONCLUSION

In conclusion, our model captures the general statistical and transient characteristics which have been observed in actual human pathological and pharmacological nerve blockades. These results indicate not only the validity of our model, but also the possibility of applying this model to clinical medicine.

ACKNOWLEDGMENTS

We thank Y. Ashkenazy, L. Safonov, and K. Kiyono for their suggestions and discussion, and K. Taura for his help with large-scale simulations. This study was in part supported by the 21st century COE program, "Information Science and Technology Strategic Core" of the Ministry of Education, Culture, Sports, Science and Technology (to K.K. and K.T.), and the Japan Science and Technology Agency (to Y.Y.).

[1] P. Bak, C. Tang, and K. Wiesenfeld, Phys. Rev. Lett. **59**, 381 (1987).
[2] J. M. Carlson and J. Doyle, Phys. Rev. E **60**, 1412 (1999).
[3] P. C. Ivanov, L. A. N. Amaral, A. L. Goldberger, and H. E. Stanley, Europhys. Lett. **43**, 363 (1998).
[4] C. K. Peng, J. Mietus, J. M. Hausdorff, S. Havlin, H. E. Stanley, and A. L. Goldberger, Phys. Rev. Lett. **70**, 1343 (1993).
[5] Y. Yamamoto and R. L. Hughson, Am. J. Physiol. **266**, R40 (1994).
[6] P. C. Ivanov, L. A. N. Amaral, A. L. Goldberger, S. Havlin, M. G. Rosenblum, Z. R. Struzik, and H. E. Stanley, Nature (London) **399**, 461 (1999).
[7] L. A. Nunes Amaral, P. C. Ivanov, N. Aoyagi, I. Hidaka, S. Tomono, A. L. Goldberger, H. E. Stanley, and Y. Yamamoto, Phys. Rev. Lett. **86**, 6026 (2001).
[8] Y. Yamamoto, Y. Nakamura, H. Sato, M. Yamamoto, K. Kato, and R. L. Hughson, Am. J. Physiol. **269**, R830 (1995).
[9] H. Seidel and H. Herzel, Physica D **115**, 145 (1998).
[10] K. Kotani, K. Takamasu, Y. Ashkenazy, H. E. Stanley, and Y. Yamamoto, Phys. Rev. E **65**, 051923 (2002).
[11] J. T. Bigger, Jr., R. C. Steinman, L. M. Rolnitzky, J. L. Fleiss, P. Albrecht, and R. J. Cohen, Circulation **93**, 2142 (1996).
[12] H. V. Huikuri, T. H. Mäkikallio, C. K. Peng, A. L. Goldberger, U. Hintze, and M. Møller, Circulation **101**, 47 (2000).
[13] J. T. Bigger, Jr., J. L. Fleiss, R. C. Steinman, L. M. Rolnitzky, R. E. Kleiger, and J. N. Rottman, Circulation **85**, 164 (1992).
[14] Z. R. Struzik, J. Hayano, S. Sakata, S. Kwak, and Y. Yamamoto, Phys. Rev. E **70**, 050901(R) (2004).
[15] N. Aoyagi, K. Ohashi, and Y. Yamamoto, Am. J. Physiol. Regulatory Integrative Comp. Physiol. **285**, R171 (2003).
[16] C. Schäfer, M. G. Rosenblum, J. Kurths, and H. H. Abel, Nature (London) **392**, 239 (1998).
[17] A. Bunde, S. Havlin, J. W. Kantelhardt, T. Penzel, J. H. Peter, and K. Voigt, Phys. Rev. Lett. **85**, 3736 (2000).
[18] F. Togo and Y. Yamamoto, Am. J. Physiol. Heart Circ. Physiol. **280**, H17 (2001).
[19] E. L. Dove and P. G. Katona, J. Appl. Physiol. **59**, 1258 (1985).
[20] R. Jung and P. G. Katona, J. Appl. Physiol. **68**, 1465 (1990).
[21] C. K. Peng, S. Havlin, H. E. Stanley, and A. L. Goldberger, Chaos **5**, 82 (1995).
[22] J. F. Muzy, E. Bacry, and A. Arneodo, Int. J. Bifurcation Chaos Appl. Sci. Eng. **4**, 245 (1994).
[23] T. Vicsek, *Fractal Growth Phenomena*, 2nd ed. (World Scientific, Singapore, 1993).
[24] Z. R. Struzik, Fractals **8**, 163 (2000).
[25] R. W. DeBoer, J. M. Karemaker, and J. Strackee, Am. J. Physiol. **253**, H680 (1987).
[26] M. G. Kienzle, D. W. Ferguson, C. L. Birkett, G. A. Myers, W. J. Berg, and D. J. Mariano, Am. J. Cardiol. **69**, 761 (1992).
[27] J. P. Saul, Y. Arai, R. D. Berger, L. S. Lilly, W. S. Colucci, and R. J. Cohen, Am. J. Cardiol. **61**, 1292 (1988).
[28] M. Elam, Y. B. Sverrisdottir, D. M. B. Rundqvist, B. G. Wallin, and V. G. Macefield, Acta Physiol. Scand. **177**, 405 (2003).
[29] R. Bannister and C. J. Mathias, in *Autonomic Failure, A Textbook of Clinical Disorders of the Autonomic Nervous System*, 4th ed., edited by C. J. Mathias and R. Bannister (Oxford University Press, Oxford, 1999), pp. 307–316.
[30] T. Schreiber and A. Schmitz, Physica D **142**, 346 (2000).